Available online at www.sciencedirect.com
ScienceDirect
Journal of Power Sources 160 (2006) 688–697
JOURNAL OF POWER SOURCES
www.elsevier.com/locate/jpowsour

Iodide-based electrolytes: A promising alternative for thermal batteries

Patrick Masset*

Karl Winnacker Institut der Dechema e.V., Theodor-Heuss Allee 25, 60486 Frankfurt-am-Main, Germany

Received 24 November 2005; received in revised form 15 December 2005; accepted 21 December 2005
Available online 28 February 2006

Abstract

Molten iodide-based salts due to their low melting points were envisaged to improve the performances of thermal batteries. Iodide-based salt drying and the determination of the basic properties (electrochemical window, conductivity, thermal heat capacity, ...) of some electrolytes were carried out. The results obtained showed that some of iodide-based electrolytes are suitable for thermal batteries. In addition, the LiF–LiCl–LiI and LiF–LiBr–KBr electrolytes were tested in Li–Si/FeS_2 single cells in the temperature of thermal battery operating conditions. The LiF–LiCl–LiI electrolyte could be considered as an interesting alternative for the improvements of thermal battery performances.

Keywords: Molten salt; Thermal batteries; Electrolyte; Iodide

1. Introduction

Thermally activated ("thermal") batteries were developed for the military purposes during the World War II as electrical generators for the V_2 missiles. At that time, the heat transferred from the "embedding system" was used as heat source to melt the salt-based electrolyte. Later, pyrotechnic compositions [1] were added. They are also very reliable, rugged and robust. As they can be stored more than 20 years without degradation, they are mainly used as electrical generators in military systems: missiles, guided bombs, shells, sub-munitions, decoys, torpedoes, aircraft security systems, One can also find applications in the area of civil high technologies (satellite [2], Ariane V launcher [3] or specific applications such as borehole generators [4]). However, thermal batteries suppliers push forward to extend their use for specific applications (operating time over one hour, pulse applications with very high power output, ...). Various technical improvements are envisaged to increase the global performances of the batteries in order to reach the future electrical needs required by the thermal batteries users. Therefore, in the last decade, numerous ways of improvements were developed:

(i) new anode using thermal spray manufacturing process of Li–Al and Li–Si alloys [5–7].
(ii) New cathode materials and manufacturing processes were studied: (Co, Ni, Fe)S_2 mixed sulfites made by hydrothermal synthesis [8], transition metal oxide-based cathode [4,9], thermal sprayed FeS_2 [10] and CoS_2-based cathodes [11]. Nevertheless, the performance benefits expected from a temperature increase are rather limited and hampered by the thermal decomposition of the pyrite.
(iii) Improvements of the insulation using vaccum multifoil design, it was shown that operation time can be maintained up to 6 h with a prototype [9,12,13].
(iv) New types of separator were developed to improve the salt retention and thinner and higher mechanical resistant separators were obtained than the usual process [14].
(v) Work was carried out at Sandia evaluating a number of iodide eutectics for possible use in thermal batteries. that work involved single-cell testing for screening purposes [15]. At the meantime, iodide-based electrolyte properties were investigated for their use in thermal batteries [16].

* Corresponding author. Tel.: +49 69 7564 362; fax: +49 69 7564 388.
E-mail address: masset@dechema.de (P. Masset).

0378-7753/$ – see front matter © 2006 Elsevier B.V. All rights reserved.
doi:10.1016/j.jpowsour.2005.12.091

It is thought that their performances (massic and volumic capacities) could be increased using electrolytes with lower temperature melting point. In this frame, it has been decided to focused our effort on low melting-point electrolytes and especially iodide-based mixtures. Earlier, iodides have been already envisaged and abandoned for their relative high cost compared to chlorides [17] and because of their hygroscopic character [18,19]. In this work, the determinations of the basic properties (electrochemical window, conductivity, heat capacity, ...) of some iodide-based electrolytes (all lithium and multi cations) were carried out in order to estimate their ability to be used as electrolytes in thermal batteries. In addition, the LiF–LiBr–KBr electrolyte (classic composition) and the LiF–LiCl–LiI electrolyte (advanced composition) were compared using a fictive load program with significant pulses added to a constant low current discharge. This article presents an overview of the results obtained and gives some indications of the future improvements in relation with iodide-based electrolytes.

2. Experimental

2.1. Chemicals

LiF, LiCl, LiBr, KCl, KBr and KI were purchased from Sigma–Aldrich (+99.99% purity). Lithium iodide 99.9% purity (- 200 mesh) was purchased from Cerac. Magnesia MgO and electrolyte and pyrite FeS_2 were used as electrolyte binder (E.B.) and cathode material, respectively. Both were furnished by ASB-Aerospatiale Batteries. Lithium–silicon alloy Li–Si (45 wt.% of lithium, 40–200 mesh) used in the anode was purchased from Cyprus Foote Mineral. High purity (+99.5%) lithium oxide Li_2O ($\leq$ 100 mesh) used in the cathode mixture comes from Cerac.

2.2. Salt, electrolyte and electrode preparation

2.2.1. Salt preparation

The salts were dried individually under vacuum in a quartz crucible for 15 h at 200 °C (473 K) according to the drying procedure established in this work (Section 3.2.1). The compositions of the electrolytes were taken from the literature [17,20–28] and reported in Table 1. The mixtures were fused under argon, in a glassy carbon crucible to prevent silica dissolution in the presence of fluoride ions, and maintained at 500 °C (773 K) for 15 h. They were quenched directly in the grinder. Once grounded, they were stored in a glove box under argon atmosphere. Impurity concentrations (mainly oxides and hydroxides) were determined to be less than 10^{-4} in the molar fraction scale. In the case of LiI, a molar fraction of 5×10^{-2} was measured.

2.2.2. Electrolyte preparation

MgO powder, used as electrolyte binder (E.B.), was provided by ASB-Aerospatiale Batteries. The MgO samples were slowly heated from room temperature to and maintained at 850 °C (1123 K) for 15 h in argon gas atmosphere. This was done to prevent hydration and carbonate formation. Appropriate amount of MgO and salt powders were accurately weighed and thoroughly mixed in a silica crucible to give about 50 g of the mixed powder in each case. The corresponding mixtures were fused for 15 h at 500 °C (773 K) in a glassy carbon crucible. As described previously for the electrolyte, they were quenched directly in the grinder. After the grinding step, they were stored under argon atmosphere in a glove-box. The grounded powders were pressed uniaxially into pellets of 35 mm in diameter and approximately 500 μm thickness.

2.2.3. Electrode preparation

From an industrial point of view, the Li–Si alloy as anode material was preferred to the Li–Al alloy. The Li–Si discharge potential is equal +157 mV versus Li^+/Li at 415 °C (683 K) [29] and then slightly lower than those of the Li–Al alloy +300 mV versus Li^+/Li at 450 °C (723 K) [29,30] which allows an increase of the power density output. Moreover, the Li–Al alloy is known to react with residual hydroxides [31,32] which could arise from the lithium iodide salt. The anode was prepared by mixing Li–Si powder with the same salt as that used in the separator. FeS_2 was used as the cathode material. The powder was sieved and particles in the 40–100 μm size range were retained. The pyrite powder was then stored under inert atmosphere in a glove-box. High purity lithium oxide was added to the catholyte as a lithiation agent. FeS_2, Li_2O and the salt powders were mixed and fused at 400 °C (673 K) for 15 h and then grinded after cooling. The anode, cathode and separator mixtures were pressed into 35 mm diameter discs under a pressure of 2000 daN cm^{-2} at room temperature. Powder processing was achieved under argon inert atmosphere to limit moisture uptake

Table 1
Melting point and composition of the molten salts electrolytes used in this study

Salts	Melting point (°C)	Weight fraction (wt.%)	Molar fraction (mol%)	References
LiF–LiCl–LiBr	443	9.6–22–68.4	22–31–47	[20]
LiF–LiBr–KBr	312	0.67–53.5–45.83	2.5–60–37.5	[21]
LiF–LiBr–KBr	312	0.81–56–43.18	3–63–34	[22]
LiF–LiCl–LiI	341	3.2–13–83.8	11.7–29.1–59.2	[23]
LiCl–KCl	354	44.8–55.2	58.8–41.2	[24]
LiI–KI	260	58.2–41.8	63.3–36.7	[25,17]
LiI–KI	280	58.2–41.8	63.3–36.7	[24,26]
LiF–LiCl–LiBr–LiI	360	4.9–11.2–34.9–49	15.4–21.7–32.9–30	[17]
LiCl–LiI–KI	265	2.6–57.3–40.1	8.5–59–32	[28]
LiCl–LiI	368	14.4–85.6	34.6–65.4	[24]

Table 2
Anode, separator S(electrolyte) and cathode weight % compositions

	Li–Si	Electrolyte	MgO	Li_2O	FeS_2
Anode	75	25	–	–	–
S(LiF–LiCl–LiI)	–	65	35	–	–
S(LiF–LiBr–KBr)	–	70	30	–	–
Cathode	–	33	–	2	65

by the salts. The weight compositions of the anode, separator and cathode are reported in Table 2.

2.3. Apparatus

2.3.1. Conductivity cell

All the experiments were driven in a glove box under high purity argon (moisture and oxygen were less than 5 ppm). The ionic conductivity cell device was made either of quartz either of boron nitride BN depending the molten salt nature. The detailled description of the cell can be found in the reference [33]. Fluorides are known to be highly corrosive against Pyrex® or quartz. Thus, boron nitride cell was used with fluoride-based salts. Earlier, hot-pressed boron nitride has been successfully used as a material for the conductance cell for molten fluorides [34,35].

2.3.2. Molten salt densities

An home made technique was used to measure the molten salt densities. The density of the molten salt was derived from the volume occupied by the molten salt. The crucibles were designed for the purpose (heigh/radius $\geq$ 10) to minimise the meniscus effect and the relative error on the height measurement. The uncertainty of the method was estimated to be less than 5%.

2.3.3. Wetting angle measurement

A small amount of salt was disposed on an 0.9 cm × 0.9 cm and 1 mm-thick MgO single crystal. It was led horizontally in a 20 mm diameter alumina cylinder. A light was disposed at the center of the tube at one of the two extremities. At the other site, a CCD-camera connected to a PC was fixed to record the pictures of the shape of the molten salt drop versus the time, the atmosphere, the temperature... The inner part of the tube was continuously maintained under a low and slightly reductive flow of hydrogenated helium (H_2 : 5 vol.%)

2.3.4. Separator deformation

Pellet-deformation tests were carried out with a modified technique described in the literature [36]. The deformation measurements consisted in the change in thickness of pellet under applied pressure. The determinations were realised at 500 °C (773 K). During the test, the pellet was held between two mica sheets. Before the test deformation, thickness of the separator and mica sheets were measured individually and together. The whole apparatus was preheated at 500 °C (773 K) for half an hour before each experiment. A constant pressure was applied for a quarter an hour and then the separator was quenched. The thickness change was determined by means of a micrometer. In the reference cited before, they measured directly the separator deformation at high temperature. In our case, all the deformation measurements were realized at room temperature. So that, our determinations might be slightly higher than the literature ones (density in the liquid state smaller than in the solid state).

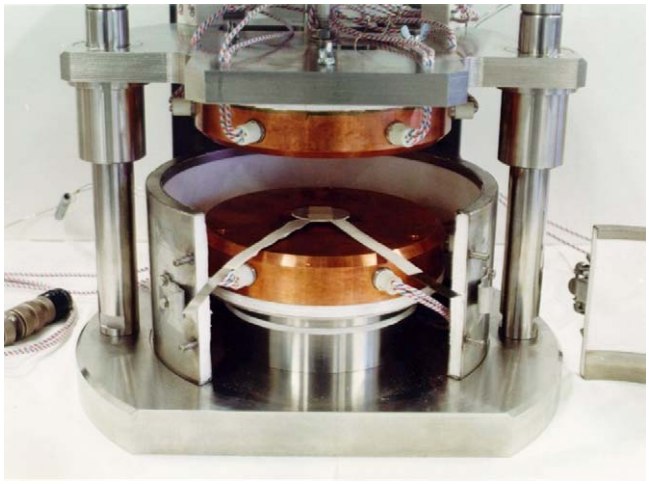

Fig. 1. Discharge test set-up.

2.3.5. Discharge test set-up

The anode/electrolyte/cathode pellets were maintained between two metallic collectors stuck onto thin mica sheets (to avoid any short-circuit with the platens) by means of a tape. Single cell discharges were performed between heated copper platens (Fig. 1). The whole apparatus was situated in a glovebox. The set-up used in this study allowed the control of the pressure applied upon the single cell. It was fixed to 0.5 daN cm^{-2}. The copper platens were pre-heated to the required temperature. As the platens temperature was correct, the cold cell was disposed between the platens and then the pressure was applied. Thus, using this procedure, the cell could reach its nominal temperature within less than 60 s. Excepted the heat-up phase, the conditions were estimated to be representative of a typical well-insulated thermal battery.

2.4. Techniques

2.4.1. Coupled differential thermal analysis (DTA)/thermogravimetry (TGA)

Thermal analyses were performed using a Setaram 24 thermal analyzer equipped with a double oven (in order to increase the TGA sensivity and stability). Experiments were carried out in dynamic atmosphere (flow rate of 125 $cm^3\ h^{-1}$) of dry helium (less than 1 ppm H_2O) on 100 mg samples. 100 ml alumina Al_2O_3 crucibles were used. Samples were prepared in glove box to prevent hydration.

2.4.2. Differential scanning calorimetry (DSC) analysis

DSC experiments were performed using a Setaram 111 thermal analyzer. Experiments were carried out in a dynamic atmosphere (flow rate of 125 $cm^3\ h^{-1}$) of dry argon (less than 1 ppm H_2O) on 150 mg samples. The crucibles were made of alumina Al_2O_3. Samples were heated from 30 to 800 °C (1073 K) at 3 °C min^{-1}.

2.4.3. X-ray diffraction (XRD)

X-ray diffraction patterns were obtained with a Siemens D500 diffractometer, using the CoKα radiation ($\lambda = 0.1789$ nm) equipped with a linear detector. X-ray diffraction was performed on samples protected by a polyethylene film to prevent a reaction with moisture.

2.4.4. Scanning electronic microscopy (SEM)

Microstructural features of the starting materials were determined by using a JEOL scanning electronic microscope. Semi-quantitative compositional were carried out by energy dispersive analysis by X-rays (EDAX) on the EDS system attached to the JEOL scanning electronic microscope. No thin films of gold on the exposed surfaces were applied before microscopic viewing. Samples were sufficiently electrical conductive and no electrostatic charging was noticed.

2.4.5. He pycnometry

MgO and salt powder densities were measured by means of helium gas pycnometry technique. The apparatus was an automatic Accupyc 1330 supplied from Micrometrics. Preliminary, samples were prepared in glove box and transferred to the analysis chamber in a closed pan in order to prevent powders hydration. Experiments were repeated three times in order to estimate the error. Dispersion of the values was less than 0.5%. Average values are given.

3. Results and discussion

3.1. Raw material characterization

3.1.1. Salt

The melting point of the electrolytes was checked by means of DSC analysis. The melting point values are reported in Table 1 and compared with the literature. Except the LiI–KI electrolyte, no discrepancy was noticed between our determinations and the literature values. The LiI–KI melting point was found to be close to 285 °C (558 K) which agrees with the data of Johnson et al. [28]. With the same mixture composition, Leiser et al. [25] proposed a value equal to 265 °C (538 K). It is thought that a water contamination could explain this difference by the formation of hydroxide and this temperature would correspond to the eutectic temperature in stable part of the reciprocal system LiI–LiOH–KI–KOH. DTA/TGA were also carried out on the mixtures to check the weight variations (before and after the drying procedure). After the drying step, no significant weight losses in the 100–200 °C range were noticed which may have been ascribed to the alkali halides hydrates decomposition. Weight losses after the drying procedure were within 0.1 wt.%. Thus, the drying procedure was considered efficient for the purpose. The specific properties needed in this study were the salt densities and thermal properties (heat capacity and heat of fusion of mixtures: see Section 3.2.3). The density measurements were realized at 25 °C and 500 °C (it corresponds to the temperature at which the deformation experiments were carried out). All the densities values are reported in the Table 3. When no data was available in the literature, a calculated value was given according to Eq. (1) with the assumption that no volume effect occurred.

Table 3
Summary of the literature and experimental values of liquid salt densities ρ(liq) at 500 °C and solid salt densities ρ(cr.) at 25 °C

Salts	ρ(cr.) (g cm^{-3})	ρ(liq.) (g cm^{-3})
LiCl–KCl	2.015 ± 0.01 (this work), 2.02⋆	1.59 ± 0.07 (this work)
LiI–KI	3.533 ± 0.018 (this work), 3.85⋆	2.83 ± 0.12 (this work)
LiF–LiCl–LiBr	2.914 ± 0.015 (this work), 2.92[16]	2.17 ± 0.09 (this work)
LiF–LiCl–LiI	3.513 ± 0.017 (this work), 3.54⋆	2.69 ± 0.10 (this work)

Values marked with the sign ⋆ are calculated values.

$$\rho = \left(\sum_i \frac{X_i}{\rho_i} \right)^{-1} \quad (1)$$

where X_i and ρ_i represent the molar fraction and the density of the constituent i in the mixture, respectively. Globally, a good agreement was found between our experimental values and published values. To our knowledge, the densities of the LiI–KI and LiF–LiCl–LiI electrolytes have been not yet determined either in the liquid or solid states. The density of the liquid state was found smaller as for the other families of halide-based electrolytes. A volume expansion occurred during the fusion of the salt which might increase the pressure of the stack in the battery. But, this volume change remains in the order of magnitude as for the other families of electrolytes.

3.1.2. MgO magnesia

Preliminary, MgO powder was studied by means of X-ray diffraction and SEM coupled with EDS analysis. It was checked that no other phases were present after the drying step. Peaks were indexed using the JCPDS file number 04829. The crystallite size was obtained by using the Debye–Scherrer relation and the half-peak broadening. Using the diffraction peak shape, the MgO crystallite size was found to be close to 45 nm. By means of SEM technique, spherical MgO particle size was determined to be close to 50 nm (Fig. 2). It agrees with the previous determination by XRD analysis.

3.1.3. FeS_2 pyrite

In the FeS_2 sample used as cathode material in discharge test, the iron, sulfur, oxygen and hydrogen contents were determined be 45.3 ± 1.8 wt.%, 56.8 ± 5.7 wt.%, 1.5 ± 0.4 wt.% and 15 ppm, respectively. By XRD, hydrated sulfates were also identified at the pyrite surface coming from the oxidation of the pyrite [37]. The composition of the pyrite was found close to $FeS_{2.25}$. Generally, this value is strongly correlated with the geographical origin of the natural mineral of pyrite. The pyrite samples were observed by MEB (Fig. 3) before and after a thermal treatment at 800 °C (1073 K). At 600 °C (873 K), the pyrite decomposes into pyrrhotite Fe_7S_8 by sulfur evolution according to Eq. (2).

$$FeS_2 \longrightarrow Fe_7S_8 + 0.43S_2 \quad (2)$$

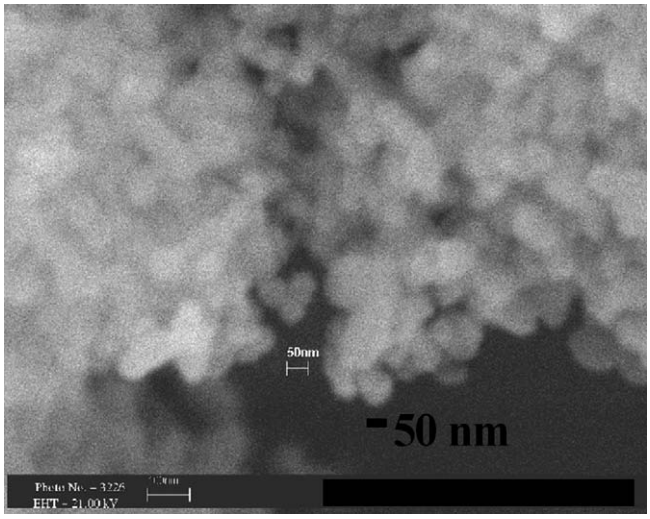

Fig. 2. MgO powder observed by SEM.

According to Eq. (2), the weight loss was close to 23% as expected and it agreed with previous studies [37–39]. The weight losses in the 500–600 °C (773–873 K) temperature range were ascribed to the thermal decomposition of sulfates [40,41]. Weight losses recorded over 700 °C (973 K) were ascribed to the thermal decomposition of the pyrrhotite Fe_7S_8 [42]. Over 600 °C (873 K), the pyrite decomposes into pyrrhotite Fe_7S_8 and sulfur gas is released in the molten salt and may react with dissolved lithium to form Li_2S in the separator [43] or oxidise the electrolyte (see Section 3.3.1). As the pyrite decomposition goes further, the pyrite becomes more and more porous from the outer surface towards the core as sulfur escapes as it is emphasized in the inset (b) in Fig. 3.

3.2. Mixtures

3.2.1. Drying procedure

Single salts used as starting materials to prepare the electrolytes may contain water coming from:

(i) water already contained at the delivery.
(ii) Water up-take during the process manufacturing.

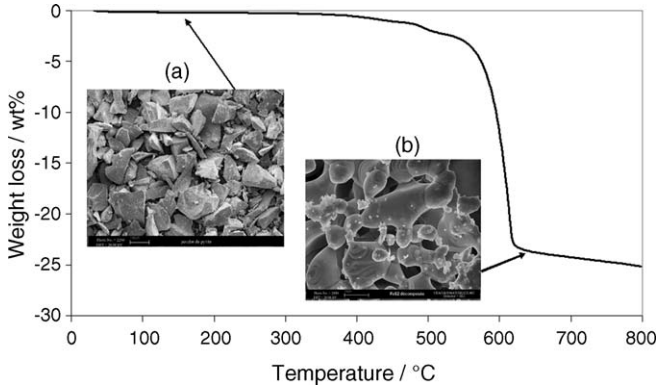

Fig. 3. TGA graph, sample FeS_2, $v = 1\,°C\,min^{-1}$, SEM observation of FeS_2 grain morphology before (a) and after (b) the thermal cycle.

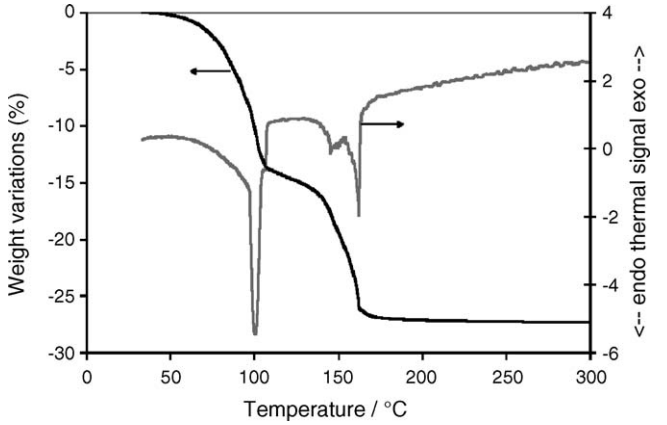

Fig. 4. Typical TGA (black line) and DTA (grey line) spectra recorded at $1\,°C\,min^{-1}$ with a sample of $LiCl{\cdot}H_2O$ hydrate.

The main objectives of the drying procedure is to remove the residual water in the salts below an acceptable level without the formation of oxide and/or hydroxide by hydrolysis. Lithium halides are known to be hygroscopic. Except lithium fluoride, it forms hydrates: LiCl [44–46] , LiBr [44,45], LiI [18,47]. To our knowledge, potassium halides do not form hydrates and are less sensitive to water up-take in dry atmosphere [48]. The dehydration temperature of each salt was checked by means of thermal analysis. It decomposes in several steps corresponding to the sub-hydrates formation (see example of $LiCl{\cdot}H_2O$ in Fig. 4). The decomposition temperatures of $LiX{\cdot}nH_2O$, (X = Cl, Br, I) hydrates and sub-hydrates were determined according to the temperature peak of the DTA and DTG signals. The uncertainty of the temperature determination was estimated to be close to ±5 °C. The temperatures are reported with literature values in Table 4. Our values agree quite well with the data published in the literature. The differences may be explained by the different experimental conditions (set-up, gas flow, . . .). On the ground of DTA/TGA measurements, the drying temperature was fixed to 200 °C. The water content was measured either by Karl–Fisher or by TG analysis (accuracy 5%). The residual amount of water was estimated to be less than 0.1 wt.% after the drying procedure (several hundreds grams dried in one batch). It was shown that iodides can be dried efficiently for the purpose of thermal batteries.

3.2.2. Oxide and hydroxide

Oxide and hydroxide come from the hydrolysis of the salts during either their synthesis or the drying procedure. Wetting tests (Fig. 5) showed that the level of oxide modifies the wetting ability of the MgO binder by the salt. Without oxide, the wetting angle of LiCl–KCl on MgO ≺ 111 ≻ single crystal was close to 56°, which agrees with previous determination [49]. By adding 1.5 mol% of lithium oxide, the wetting behavior was strongly modified because the wetting angle decreased down to 30°. Therefore, the oxide formation during the drying procedure should be be controlled carefully in order to keep or improve the wettability of the MgO binder by the salt. The global amount of oxide and hydroxide in the salt was evaluated by pH titration. A small amount of salt (1–2 g) was dissolved in deionized water

Table 4
Decomposition temperature of $LiX \cdot nH_2O$ hydrates (X = Cl, Br, I) under helium atmosphere (25 $cm^3\ h^{-1}$) determined by thermal analysis

LiX	$n = 3$	$n = 1$	$n = 0.5$
LiCl	–	98 (this work), 110 [45]; 100.5 [44], 99 [46]	160 (this work), 162 [45]; 152 [44]
LiBr	–	160 (this work), 110 [45]	175 (this work), 165 [45]; 159 [44]
LiI	190 (this work), 210 [47]	215 [47]	–

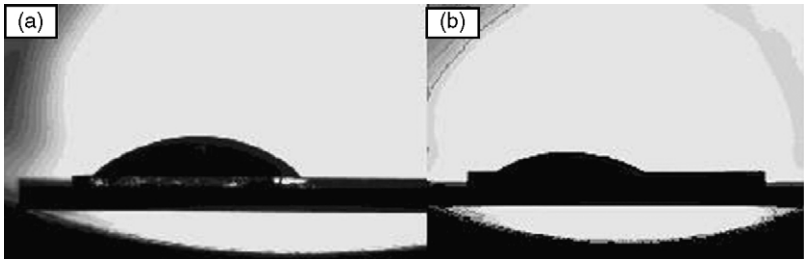

Fig. 5. Pictures of the shape of a drop of molten salt on a MgO single crystal at 425 °C (733 K) under He (5 vol.% H_2) atmosphere, (a) LiCl–KCl eutectic, (b) LiCl–KCl eutectic (1.5 mol% Li_2O).

Table 5
Heat capacity C_p ($J\ K^{-1}\ g^{-1}$) and heat of fusion ΔH_{fusion} ($J\ K^{-1}\ g^{-1}$) of the electrolytes

Salts	C_p(cr.) T_f ($J\ K^{-1}\ g^{-1}$)	C_p(liq.) − C_p(cr.) @ T_f ($J\ K^{-1}\ g^{-1}$)	ΔH_{fusion} ($J\ g^{-1}$)	ΔH_{fusion}(liter) ($J\ g^{-1}$)
LiCl–KCl	0.74	0.26	244 ± 8	234.78 [51,1]
LiI–KI	0.55	0.85	71 ± 2	–
LiF–LiCl–LiBr	0.87	0.41	266 ± 9	293.70 [51,1]
LiF–LiCl–LiI	1.22	nd⋆	157 ± 5	–
LiF–LiBr–KBr	0.505	0.248	103 ± 3	134 [51,1]

and the amount of oxide plus hydroxide was derived from the pH variation. Nevertheless, it should be pointed out that, using this method, the oxide and hydroxide concentrations cannot be determined separately. Only, a global value was obtained. In the case of LiI, a molar fraction of 5×10^{-4} was measured. It corresponds to the original content of LiOH in the salt. By DTA, a weak peak was detected at 271 °C (544 K), corresponding to the liquidus temperature of the LiI–LiOH binary mixture [50]. Otherwise, the impurity concentrations (oxide plus hydroxide) were determined to be less than 10^{-4} mole fraction. By coupling pH and LECO measurements, the oxides and hydroxides concentrations can be determined separately. This measurement requires working cleanly to ovoid any cross-contamination by the residual water or/and oxygen that may interfere in the concentration determination. The level of oxide + hydroxide was checked at each step of the electrolyte manufacturing. It was found that the level of oxide + hydroxide remained constant before and after the drying procedure.

3.2.3. Thermal properties of the electrolytes

The thermal properties of LiI–KI and LiF–LiCl–LiI iodide-based electrolytes have been determined for the engineering of the thermal batteries. The heat capacities, heat of fusion measured in this work are reported in Table 5 and compared with those of the classical electrolytes, e.g. LiCl–KCl, LiF–LiCl–LiBr [51,52]. The heats of fusion of iodide-based electrolytes were found lower than those of the classical electrolytes. It might be ascribed to the radius of the iodide anion, which diminishes the crystal stability, and, then less energy is required to melt the crystal. For the LiF–LiCl–LiI electrolyte, the heat capacity was found to be higher compared to all of the electrolytes.

3.2.4. Separator deformation

Deformation tests on separators (electrolyte + MgO) were carried out at 500 °C (773 K) whereas it was applied a pressure equal to 0.45 daN cm^{-2} with a modified technique described in the literature [36]. The deformation measurements consisted in the change in thickness of pellet under applied pressure. It was shown that a 27–30 vol.% of magnesia was found to be enough to obtain an efficient retention whatever the electrolyte nature. Optimum values are reported in Table 6. For LiF–LiCl–LiI, it was found that 30–35 wt.% of MgO was correct. This value agrees with the value proposed in the literature [15].

3.3. Electrochemical determinations

3.3.1. Electrochemical window

As shown previously (Section 3.1.3), sulfur is released in the molten salt during the operating time of the battery. Despite the

Table 6
Summary of the optimum volume and weight fractions Ψ_{MgO} of magnesia

	LiCl–KCl	LiF–LiCl–LiBr	LiI–KI	LiF–LiCl–LiI
Ψ_{MgO} (wt.%)	45	40	35	32.5
Ψ_{MgO} (vol%)	27.2	29.4	30.3	27

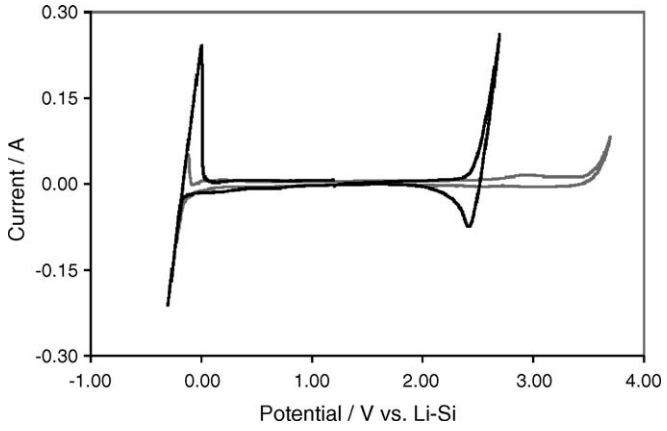

Fig. 6. Voltammogramms in LiCl–KCl (grey line) and LiF–LiCl–LiI bath (dark line), $T = 425\,^{\circ}C$, $v = 0.25\,V\,s^{-1}$, working and counter electrodes : W wires, reference electrode: Li–Si alloy.

low solubility of pyrite and pyrrhotite [53] in the molten salt, sulfur issued from the thermal decomposition of pyrite may react with the polysulfides (S_n^{2-}) arising from the dissolved pyrite to form polysulfites (S_n^{-}) [54,55]. By cyclic voltammetry (Fig. 6), the electrochemical windows of iodide-based electrolytes were determined. Lithium deposit potential was found to be close to −160 mV versus Li–Si at 425 °C (698 K) that agrees with the data from Sharma et al. [53]. Moreover, it was found unchanged in the iodide-based electrolytes like the Li–Al alloy behaves in different electrolytes [30]. The most oxidizable halide was found to be the iodide. Its oxidation potential was found to be around 2.55 V versus Li–Si reference at 425 °C (698 K), which is around 1 V lower than with pure chloride-based electrolytes (Fig. 6). This value is correct regarding the value of 3.14 V versus Li^+/Li at 450 °C (723 K) of the standard potential of the I_2/I^- redox couple given by Plambeck [56]. At 460 °C (733 K), the redox potentials of the pyrite-based system, dissolved sulfides and polysulfites are close to 1.95, 2.35 and 2.5 versus Li–Si [57], respectively. The electrolyte should be stable even though the presence of sulfur, polysulfide or/and polysulfite species. Therefore, the presence iodide in the electrolyte does not preclude its use for thermal batteries.

3.3.2. Ionic conductivity

Lowering the melting point of the electrolyte seems to be interesting to reduce the thermal decomposition of pyrite by decreasing the upper temperature limit. But on the other hand, one question remains uncertain: does the load program could be sustained at low temperature, especially near the melting point or at the end of life of the battery ? Different iodide-based compositions were tested and compared with other classical electrolytes. The ionic conductivities of all lithium iodide-based electrolytes were found higher than the other ones [33]. This is mainly due to the higher ionic mobility of the lithium cation compared to that of potassium. Concerning the classical compositions our results agree with the previous determinations published in the literature (LiCl–LiI, LiI–KI [58], LiCl–KCl [58,21], LiF–LiCl–LiBr [58,21], LiF–LiBr–KBr [58,21], . . .). To our knowledge, no data concerning the ionic conductivity of LiF–LiCl–LiI (except one value 2.3 $S\,cm^{-1}$ at 375 °C [59]) was published. The ionic conductivities of numerous iodide-based electrolytes have been investigated. It appeared that most of them were not suitable for the thermal battery application which requires current peaks at the end of the battery life. Opposite, the advanced composition LiF–LiCl–LiI seems to be promising and suitable to be used in thermal batteries. The ionic conductivity of the LiF–LiCl–LiI electrolyte was fully measured in the 345–600 °C (613–873 K) temperature range and it could be expressed as a function of temperature as follows: $\sigma = 8.8995 \exp(-872.6/T(K))$ in $S\,cm^{-1}$.

3.4. Discharge tests

To complete the basic determinations, a comparative single cell discharge study of two electrolytes: LiF–LiBr–KBr and LiF–LiCl–LiI. These two electrolytes were selected because their melting points are close. Therefore, performance output can be compared easily. Single cell discharges were carried out in the 400–580 °C (673–853 K) temperature range that corresponds approximately to the operating temperature of the thermal batteries. A fictive load program was applied to measure the cell performances. The load program contained:

(i) a steady-state current of 25 mA cm^{-2} was applied throughout the experiments, which stimulates the continuous electrical needs during the life of the battery.
(ii) Every 120 s, short current pulses of 1 A cm^{-2} were imposed in order to measure the internal cell resistance during the discharge.
(iii) After 1860 s and 2860 s, current pulses of 500 mA cm^{-2} were applied during 30 s, which corresponds to the electrical needs that might be required at the end of the battery life.

Prior to discharge, a delay of 60 s was observed to make sure that the cell had reached the required temperature. It was considered that the cell potential of the cell should remain higher than 1.6 V during the discharge and especially during the long pulses. As shown in Fig 7, the LiF–LiBr–KBr-based cells could not sustain the load program at temperatures lower than 460 °C. It was the most important difference noticed between the performances of the two electrolytes studied. With the iodide-based electrolyte and at low temperature ($T \leq 450\,^{\circ}C$), the cathode efficiency was close to unity. Conversely, with the LiF–LiBr–KBr electrolyte, the cathode efficiency was found to be rather low at temperatures below 450 °C. This was ascribed to the poor conductivity of this electrolyte and the high internal cell resistance induced. Therefore, the second discharge plateau was shorter than expected. At temperatures higher than 550 °C, one can observe a very similar behaviour for both electrolytes, with a decrease of the cathode efficiency mainly due to the thermal decomposition of pyrite. The kinetics of this thermal decomposition was investigated in molten salts LiX–KX (X = Cl, Br, I) [39]. The LiF–LiBr–KBr (0.7–53.5–45.83 mol%) molar composition is close to that of LiBr–KBr (60–40 mol%). It was shown that the pyrite decomposition rate was a few percents higher in LiF–LiCl–LiI than in

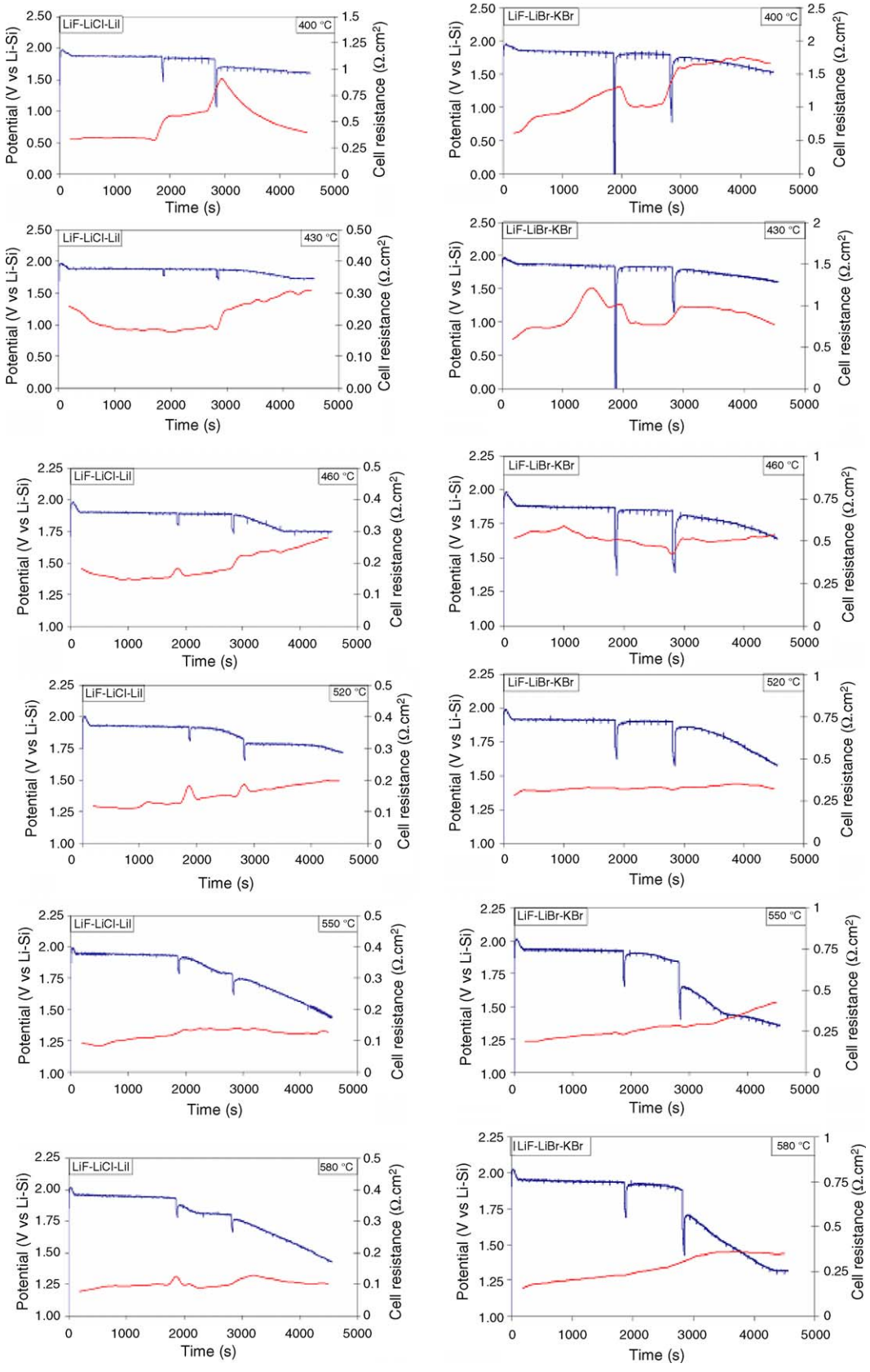

Fig. 7. Cell voltage (dark line) and cell resistance (gray line) vs. time of Li–Si/FeS_2 cells, (a) LiF–LiBr–KBr electrolyte, (b) LiF–LiCl–LiI between 400 and 550 °C.

LiBr–KBr. The measured cathode efficiency agreed with previous kinetic determinations that we made elsewhere. Our results agree also with the data published by Guidotti et al. [15]. They found that cathode efficiency decreased drastically with the use of iodide-based electrolytes at high temperatures with respect to the all-lithium LiF–LiCl–LiBr electrolyte. We observed a similar behaviour for both electrolytes. In conclusion, we can state that the efficiency of FeS_2 is severely reduced at high temperatures both in the LiF–LiBr–KBr and in the all-lithium LiF–LiCl–LiI electrolyte. Temperature should be carefully controlled (pyrotechnics and insulators) and should do not exceed 600 °C for long time operation. We examined the cell internal resistance, on which the voltage of operating cells depends. The overall resistance of the LiF–LiBr–KBr based cells was found twice higher than that of the iodide based cells whatever the temperature. The variations with temperature were mainly linked to the variations of the electrolyte ionic conductivity, whereas its time evolution during a given discharge process was affected by phase precipitation.

3.5. Future for iodide-based electrolytes

This work showed that iodide salts are more sensitive to moisture than chlorides, which complicates their handling at the industrial scale and may require their handling under inert atmosphere for long manufacturing process. But, it has been established that iodide-based electrolytes, and especially the LiFLiCl–LiI eutectic, are suitable as electrolyte in thermal batteries. And it has also been proved that lowering the operating temperature range of the thermal batteries by using iodides remains interesting. Therefore, the iodide-based electrolytes still represents a way of progress. The advantages of the all-litihum LiF–LiCl–LiI electrolyte composition are well identified:

(i) the risk of precipitation phenomenon in the alloy-based anode [60] and the concentration gradient [61] at the electrodes during current peaks is reduced.
(ii) The ionic conductivity is enhanced. The drawback of all-lithium electrolyte is that the first plateau efficiency decreases inversely proportionally with the lithium activity in the electrolyte [62].

By comparison with the LiF–LiCl–LiBr which operates at temperature over 450 °C, or the LiF–LiBr–KBr which can sustain a load program only above 450 °C [63], it is thought that the lower limit of the operating temperature of the iodide-based electrolyte could be increased without reducing drastically the performances of the battery. Preserving the advantages of the all lithium iodide-based electrolyte, it thought that substituting partially LiI by LiF and LiCl in the ternary mixture, the rate of the thermal decomposition of the pyrite would be reduced [64]. Moreover by decreasing the iodide content in the electrolyte the sensibility of the solid salt against moisture would be also reduced [48]. According to the LiF–LiCl–LiI phase diagram (Fig. 8), moving the composition of the ternary mixture along the eutectic valley to cross the dashed lines superimposed to the phase diagram gives two compositions C_{400} and C_{450} at 400 and 450 °C, respectively. The composition C_{400} is equal 20–40–40 mol% whereas the C_{450} is close to 25–55–20 mol%.

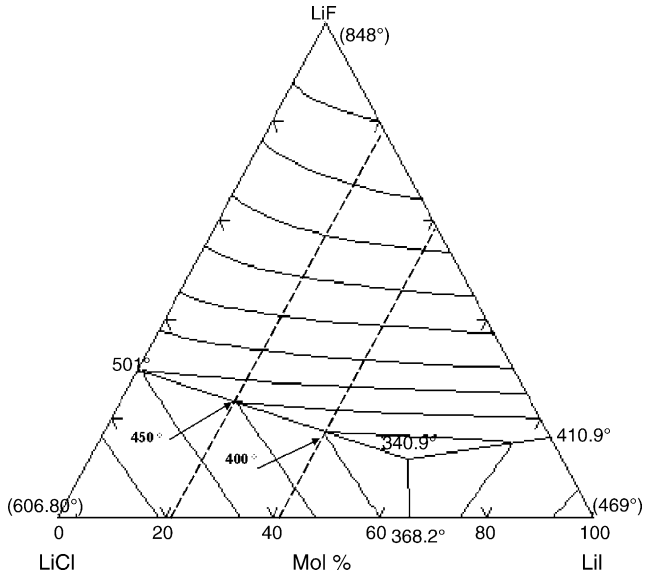

Fig. 8. LiF–LiCl–LiI phase diagram.

4. Conclusions

In this work, iodide-based electrolytes were investigated. Despite their sensibility against moisture, it was shown that some of them are suitable to be used as electrolytes in thermal batteries. It was demonstrated that iodide-based electrolyte can be handled efficiently from the delivery until the end of the manufacturing process with accurate control tools. The selected composition LiF–LiCl–LiI was tested and compared with the classical composition LiF–LiBr–KBr electrolyte with discharge tests. The results showed that the output performances are at least equal at high temperture (above 450 °C) and better below 450 °C. Considering the ternary composition LiF–LiCl–LiI, it is thought that the modification of the composition might reduce its sensibility against moisture and reduce the FeS_2 decomposition rate. Therefore, an increase of the performances is still expected with this advanced composition.

Acknowledgments

This article is a summary of the thesis (1999–2002) of Patrick Masset which acknowledges the financial support of the CEA Le Ripault, ASB-Aerospatiale Batteries and LEPMI. Serge Schoeffert from ASB-Aerospatiale Batteries, Jean-Yves Poinso from CEA Le Ripault and Jean-Claude Poignet from LEPMI are deeply thanked for their continuous support and guidance during the course of this project. However, the content of the text is of the only responsability of the author and that does not represent the thought of the persons and institutions cited above.

References

[1] R.A. Guidotti, Proceedings of the 27th International Sample Technical Conference, 1999.
[2] S. Kaufmann, S. Chagnon, Proceedings of the 35th International Power Sources Symposium, 1992, p. 227.
[3] B.P. Dagarin, R.K. Taenka, E.J. Stofel, IEEE Aerosp. Electectron. Syst. Mag. 11 (6) (1996) 6.
[4] R.A. Guidotti, F.W. Reinhardt, Proceedings of the 38th Power Sources Conference, 1998, p. 470.
[5] C.L. Crowley, N.A. Elkouh, C. Lamb, Proceedings of the 39th International Power Sources Conference, 2000, p. 517.
[6] C.L. Crowley, N.A. Elkouh, C. Lamb, Proceeding of 40th International Power Sources Conference, 2000, p. 303.
[7] E. Raub, C.L. Crowley, N.A. Elkouh, C. Lamb, Proceedings of the 40th International Power Sources Conference, 2000, p. 307.
[8] R.A. Guidotti, F.W. Reinhardt, Proceedings of the 39th Power Sources Conference, 2000, p. 487.
[9] R.A. Guidotti, F.W. Reinhardt,. Proceedings of the 40th Power Sources Conference, 2002, p. 250.
[10] D.E. Reisner, et al., Proceedings of the 17th International Seminar Exhibition on Primary and Secondary Batteries, 2000.
[11] R.A. Guidotti, J. Dai, T.D. Xiao, D.E. Reisner, Proceeding of the 15th Annual Battery Conference, Long Beach, CA, 2000, p. 127.
[12] T.D. Kaun, P.A. Nelson, Proceedings of the 39th International Power Sources Conference, 2000, p. 483.
[13] R.A. Guidotti, F.W. Reinhardt, Proceedings of the 40th Power Sources Conference 2002, p. 299.
[14] T.D. Kaun, M.C. Hash, H. Norris, Proceedings of the 40th Power Sources Conference, 2002, p. 291.
[15] R.A. Guidotti, F.W. Reinhardt, Proceedings of the ECS 211th Meeting, Philadelphia, 2002.
[16] J.-Y. Poinso, M.-H. Poinso, A. Henry, Proceeding of the 39th International Power Sources Conference, 2000, p. 491.
[17] W. Borger, D. Kunze, H.S. Panesar, Prog. Batt. Sol. Cells 4 (1982) 258.
[18] Chevalier, CNAM Report, Speciality “Electrochemistry”, 1988 pp. 12–34 (in French).
[19] M.E. Melnichak, O.J. Kleppa, J. Chem. Phys. 52 (4) (1970) 1790.
[20] A.G. Bergman, A.S. Arabadshan, Russ. J. Inorg. Chem. 8 (5) (1963) 369 (English Translation).
[21] L. Redey, R.A. Guidotti, Proceedings of the 37th Power Sources Conference, 1996, p. 255.
[22] L. Redey, M. McParland, R. Guidotti, Proceeding of 34th International Power Sources Conference, 1990, p. 128.
[23] C.E. Johnson, J.E. Hathaway, J. Chem. Eng. Data 14 (2) (1969) 174.
[24] J. Sangster, A.D. Pelton, J. Phys. Chem. Ref. Data 16 (3) (1987) 509.
[25] D.B. Leiser, O.J. Whittemore Jr., J. Am. Ceram. Soc. 50 (1) (1967) 60.
[26] R. Sridhar, C.E. Johnson, E.J. Cairns, J. Chem. Eng. Data 15 (2) (1970) 244.
[27] A.G. Bergman, S.I. Berezina, E.L. Bakumskaya, Russ. J. Inorg. Chem. (1963) 1122 (English Translation).
[28] C.E. Johnson, M.S. Foster, J. Electrochem. Soc. 116 (11) (1969) 1612.
[29] C.J. Wen, R.A. Huggins, J. Sol. St. Chem. 37 (1981) 271.
[30] N.P. Yao, L.A. Heredy, R.C. Saunders, J. Electrochem. Soc. 118 (7) (1971) 1309.
[31] A.I. Demidov, P.V. Gavrilov, Russ. J. Appl. Chem. 71 (8) (1998) 1310.
[32] J.Y. Poinso, Proceedings of the EUCHEM (Porquerolles, Fr.), 1998.
[33] P. Masset, A. Henry, J.-Y. Poinso, J.-C. Poignet, J. Power Sources 160 (2006) 752–757.
[34] E.W. Yim, M. Feinleib, J. Electrochem. Soc. 104 (2) (1957) 622.
[35] E.W. Yim, M. Feinleib, J. Electrochem. Soc. 104 (2) (1957) 626.
[36] R.A. Guidotti, F.W. Reinhardt, Sandia National Laboratories, 1985.
[37] J.P. Pemsler, et al., J. Electrochem. Soc. 137 (1) (1990) 1.
[38] S. Dallek, B.F. Larrick, Thermochim. Acta 95 (1985) 139.
[39] P. Masset, S. Schoeffert, J.-Y. Poinso, J.-C. Poignet, Proceedings of the 40th Power Sources Conference, 2002 p. 246.
[40] P.K. Gallagher, D.W. Johnson, F. Schrey, J. Am. Ceram. Soc. 53 (12) (1970) 666.
[41] P. Masset, J.-Y. Poinso, J.-C. Poignet, J. Therm. Anal. Cal., in press.
[42] I.C. Hoare, et al., J. Chem. Soc. Faraday Trans. 1 84 (9) (1988) 3071.
[43] M.C. Hash, et al., Proceedings of the International Symposium on Molten Salts, 1992.
[44] G.F. Huttig, W. Steudemann, Z. Phys. Chem. 126 (1–2) (1927) 279.
[45] M. Manewa, H.P. Fritz, A. Anorg. allg. Chem. 296 (3) (1973) 279.
[46] W. Voigt, D. Zeng, Pure Appl. Chem. 74 (10) (2002) 1909.
[47] K. Rudo, P. Hartwig, W. Weppner, Rev. Chim. Miner. 17 (4) (1980) 420.
[48] P. Masset, J.-Y. Poinso, J.-C. Poignet, J. Power Sources 137 (2004) 140.
[49] J.G. Eberhardt, Argonne National Laboratories, 1979.
[50] P. Hartwig, et al., Z. Anorg. Allg. Chem. 518 (1984) 137.
[51] R.A. Guidotti, F.W. Reinhardt, Proceedings of the 33rd International Power Sources Conference, 1988.
[52] R.A. Guidotti, F.W. Reinhardt, J. Power sources 15 (1995) 43.
[53] R.A. Sharma, R.N. Seefurth, J. Electrochem. Soc. 131 (5) (1984) 1084.
[54] F.G. bodevig, J.A. Plambeck, J. Electrochem. Soc. 117 (7) (1970) 904.
[55] D.M. gruen, R.L. McBeth, A.J. Zielen, J. Am. Chem. Soc. 93 (24) (1971) 6691.
[56] J.A. Plambeck, Fused salts systems, in: Marcel Dekker Inc. (Ed.), Encyclopedia of Electrochemistry of Elements, vol. X 1976.
[57] J.R. Birk, R.K. Steunenberg, New use of sulfur, In: J.R.W. Editor (Ed.), Advances in Chemistry, Series 140. ACS, 1975.
[58] G.J. Janz, J. Phys. Chem. Ref. Data 17 (2) (1988) 309.
[59] R.C. Vogel et al., Chemical engineering division annual report, ANL Report-7775, 1971 p. 120.
[60] C.E. Vallet, et al., J. Electrochem. Soc. 130 (12) (1983) 2370.
[61] J. Braustein, C.E. Vallet, J. Electrochem. Soc. 126 (6) (1979) 960.
[62] S.S. Wang, R.N. Seefurth, J. Electrochem. Soc. 143 (3) (1987) 530.
[63] P. Masset, S. Schoeffert, J.-Y. Poinso, J.-C. Poignet, J. Electrochem. Soc. 152 (2) (2005) 405.
[64] P. Masset, V. Frotté, J.-Y. Poinso, J.-C. Poignet, in preparation.